

Improving automatic feature detection from LIDAR intensity by integration of LIDAR height data and true orthoimage from digital camera

LAMYAA GAMAL EL-DEEN TAHA SOLYMAN

Abstract—Airborne laser scanning (ALS) and multispectral photography have synergic capabilities for information extraction. Feature detection methodologies are very important in the context of spatial data capture and updating for GIS applications. These methodologies can be based on either LIDAR data or photogrammetric data or even on a combination between them. True orthoimages were generated by orthorectification of digital camera images using DSM from LIDAR data. Leica Photogrammetric Suite (LPS) module of Erdsa Imagine 9.2 software was utilized for processing.

Several classifications based on supervised maximum likelihood classifier were conducted on the five different datasets.

The first classification was performed using the intensity image. The second classification was performed using three digital aerial image channels. The third classification was performed using the three digital aerial image channels and two LIDAR feature images (average and standard deviation). The fourth classification was performed using two LIDAR feature images. The last classification was performed using the three digital aerial image channels combined with intensity metric and two LIDAR feature images (average and standard deviation). Quantitative accuracy assessments of the classification results were performed. A comparison between these five approaches has been carried out. After that morphological operations were performed in order to remove noise.

The results revealed that the last approach is the best followed by the third approach then the second approach then the fourth approach followed by the first approach.

The last approach result has been improved by applying neural network classification. ENVI 4.8 software was utilized for this purpose. The overall accuracy was 97%, and kappa coefficient was 0.94. It was found that the neural network classification gives better classification accuracy than maximum likelihood classification.

The results of the best approach of the maximum likelihood classification (fifth) and the results of the neural network classification were compared with those obtained using only information from the intensity image and showed an increase in accuracy of land-use discrimination up to 35% and 36.7%, respectively.

Manuscript received April 29, 2012. This work was financially supported by National Authority of Remote Sensing and Space Science.

The Author is with the National Authority of Remote Sensing and Space Science, Cairo, Egypt (phone: 202- 26251265; fax: 202-26225800; e-mail: Lamyaa@narss.sci.eg

Keywords— Digital photogrammetric camera, Digital photogrammetric workstations, Feature detection, Lidar intensity, Lidar metric , Neural network , Raw lidar data , True orthoimage.

INTRODUCTION

Urban Land use land cover information is essential for planning, urban development, emergency management and monitoring the environment. The land-cover information extraction from remote sensing imagery, however, is a difficult task depending on the complexity of the landscape and the spatial and spectral resolution of the imagery. Improving the accuracy of land-cover classifications is thus a fundamental research topic [15].

Aerial images and Light Detection And Ranging (Lidar) data are common sources for feature extraction. In digital photogrammetry, features of objects are extracted using 3D information from image matching or DSM/DTM data, spectral, textural and other information sources [1].

LIDAR provides very accurate position and height information, but less direct information on the geometrical shape of objects within the field of view. High-resolution imagery on the other hand offers very detailed information on object attributes, such as spectral signature, texture and shape [6]

Raw LIDAR data derived from LIDAR pulse returns is known as a point cloud [21]. In addition to the X, Y and Z triplets, LIDAR systems are able to record the intensity of the returns, which is a measure of the amount of energy reflected back to the sensor. The intensity recorded by LIDAR systems is a function of many variables such as laser power, incidence angle, target reflectivity and area, atmospheric absorption and the range (sensor target distance) [12]

Classifications have until recently been attempted with multispectral imagery.

LIDAR intensity information has not been greatly used either in the commercial sector or in academia, yet it could be an important factor for feature extraction or land cover classification [13]. LIDAR intensity images often appear heterogeneous and speckled, due to the excessive noise and artefacts caused by the sensor scanning. The main source of intensity noise is the angle of reflection, as some land covers

have different intensity values as the angle of reflection varies [20].

To enhance the quality of the intensity data classification, some studies have been conducted by incorporating ancillary data [14].

Digital photogrammetric cameras can capture high dynamic images at a good signal-to-noise ratio. Compared to the use of scanned analogue images, these features are especially advantageous with respect to the accuracy, reliability and density of automatic point transfer [2]. The main advantages of digital aerial cameras over their analogue counterparts are a completely digital data flow line, a significantly improved radiometric image quality, together with the possibility to simultaneously acquire panchromatic, colour and near-infrared imagery[3].

Direct georeferencing has become more and more popular in the last decade. Direct georeferencing is mainly used for orthophoto production. With high resolution images an aerotriangulation is still mandatory because the sub-pixel precision potential of the high resolution images cannot be achieved with direct georeferencing [4], [5].

Photogrammetry and LIDAR have their unique advantages and drawbacks for feature extraction [6].

Quite some efforts have been spent in the past to automatically extract feature from digital aerial images or from digital surface models (DSM) derived from laser scanner data. The most recent achievements in the field of automated acquisition of features are based on the integration of data from two or more sources in order to overcome the drawbacks of specific sensor types. In this research feature detection has been performed based on two supervised classifiers, maximum likelihood and neural network.

Maximum likelihood classification was performed using five different data sets (approaches).

1) intensity image, 2) true Orthomosaic resulted from orthorectification of digital camera images using DSM from LIDAR data (the three digital aerial image bands), 3) true orthomosaic from digital camera (the three digital aerial image bands) combined with height metrics (average and standard deviation), 4) height metrics alone (average and standard deviation), and 5) height metrics combined with intensity metric and true Orthomosaic from digital camera.

Neural network was performed using the fifth data sets

II. STUDY AREA AND DATA SET

The data used in this paper are free sample data for Vaihingen/Enz, Germany, kindly provided by the International Society of Photogrammetry and Remote Sensing (ISPRS) commission III -working group III / 4 (area2). Aerial measurements with laser scanner and digital camera were made. The images were taken with a large-format frame camera (Intergraph / ZI DMC) from an altitude of 900 m above ground on 24 July and 6 August 2008. The focal length

of the camera 120 mm and the coordinates of principal point (0,0) In total, the block consisted of five overlapping strips with two additional cross strips at both ends of the block. The test area is visible in two of these strips, namely strips 4, and 5. The aerial image used here is a 3 channel (RGB) image with 8 cm ground sampling distance (GSD). The forward overlap is 60%. A set of orientation parameters, determined by the Institute of Photogrammetry, University Stuttgart were provided with the images (Cramer, 2010) Table 1 indicates the exterior orientation of the digital images of the Vaihingen Block.

The LIDAR data were extracted from laser scanning data generated using Leica ALS50 system with 45° field of view and a mean flying height above ground of 500m. The average strip overlap is 30%, and the median point density is 6.7 points / m². Point density varies considerably over the whole block depending on the overlap, but in regions covered by only one strip the mean point density is 4 points / m². The original point clouds were post-processed by strip adjustment to correct for systematic errors in georeferencing. In this process, object planes derived from the 8 cm DMC block were used as ground control, so that the georeferencing of the ALS data is consistent with the exterior orientation of the DMC images. As a result of the strip adjustment, the standard deviation derived from the median of absolute deviation in the overlap.

The test area is visible in five of LIDAR strips, namely strips 3,5,7,9,10

Table 1 Exterior orientation of the digital images of the Vaihingen Block.

Strip	Image file	Projection Centres			Rotation Angles (w: primary, x: secondary, y: tertiary, z)		
		X ₀ [m]	Y ₀ [m]	Z ₀ [m]	φ	ω	κ
4	1004_0081.tif	4965.58.488	5419.884.008	118.1.985	-0.8709	-0.3652	-199.2010
4	1004_0082.tif	4968.04.479	5419.882.183	118.3.373	-0.2693	-0.6381	-198.97290
4	1004_0083.tif	4970.48.699	5419.882.847	118.4.616	-0.3483	-0.4017	-199.44720
4	1004_0084.tif	4972.96.587	5419.884.550	118.5.010	-0.8150	-0.5302	-199.36600
5	1005_0103.tif	4965.73.369	5419.477.807	116.1.431	-0.4828	-0.0310	-0.23869
5	1005_0104.tif	4968.17.972	5419.478.832	116.1.408	-0.6521	-0.0631	-0.17326
5	1005_0105.tif	4970.64.985	5419.478.830	115.9.940	-0.7465	-0.1188	-0.09710
5	1005_0106.tif	4973.12.996	5419.477.088	115.8.888	-0.5345	-0.1902	-0.13489

III. METHODOLOGY

- Photogrammetric project creation has been

performed in digital photogrammetric workstation Leica Photogrammetric Suite (LPS) module of Erdsa Imagine 9.2 software.

- Digital aerial images (RGB) taken with a large-format frame camera (Intergraph / ZI DMC) have been imported.
- Image pyramids have been performed.
- Interior orientation parameters and exterior orientation parameters were defined.
- True Orthoimage were generated by true orthorectification of digital camera images using DSM from LIDAR data. Leica Photogrammetric Suite (LPS) module of Erdsa Imagine 9.2 software was utilized for true orthoimage generation.
- Radiometric qualization of true orthoimages have been made.
- Image mosaicking has been performed.
- Lastools software was used for merging raw LIDAR data (.las files of LIDAR strips) .
- Lastools software was used for derivation of LIDAR metrics (intensity, average , and standard deviation).
- Filtering the noise of intensity image has been performed.
- Subsetting of the intensity images, average, and standard deviation.
- Coregistrtion of the different feature sets.
- Maximum likelihood classifier has been used for feature detection. Classification was performed using five different approaches. In the first approach, classification was performed using the intensity image while in the second approach, classification was performed using the three digital aerial image channels whereas in the third approach, classification was performed using the three digital aerial image channels and two LIDAR feature images(average and standard deviation). In the fourth approach, classification was performed using two LIDAR feature images (average and standard deviation). In the last approach, classification was performed using a combination of three digital aerial image channels, intensity image and two LIDAR feature images (average and standard deviation).
- Accuracy assessment of classifications was carried out using overall accuracy and kappa coefficient. Seventy randomly selected points were used for this purpose.
- Morphological operations were performed in order to remove noise.
- The last approach result has been improved by applying neural network. ENVI 4.8 software was utilized for this purpose.
- Accuracy assessment of neural network classification was carried out using overall accuracy and kappa coefficient.

A. Photogrammetric project creation

Photogrammetric project creation means establish a coordinate system, datum and ground units for the project. A project was created to include digital camera images. Leica Photogrammetric Suite (LPS) module of Erdsa Imagine 9.2 software was utilized for processing. Fig.1 shows block configuration.

Interior orientation parameters and exterior orientation parameters were defined.

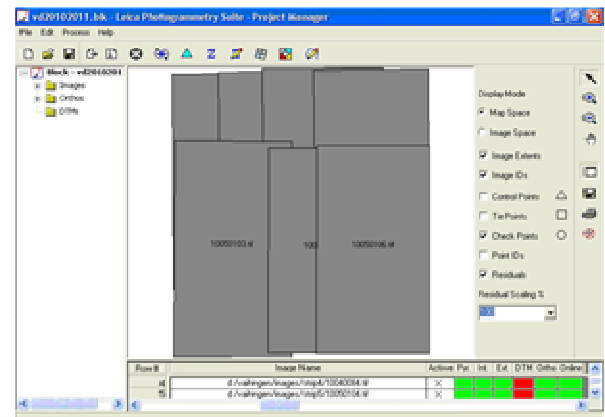


Fig.1 Block configuration.

B. Digital surface model (DSM)

Airborne LIDAR is a potential data source for providing height information (DSM or DTM).

Digital surface model (DSM) includes any buildings, vehicles, vegetation (canopy and understory), as well as the "bare ground". To generate the required "bare-earth Digital Terrain Model (DTM), ground and non-ground features/data points must be distinguished from each other so that the latter can be eliminated before DTM building [6] .

Fig.2 shows Lidar DSM of the study area. Fig3. illustrates height variation in Lidar DSM of the whole LIDAR survey.



Fig2. Lidar DSM of the study area.

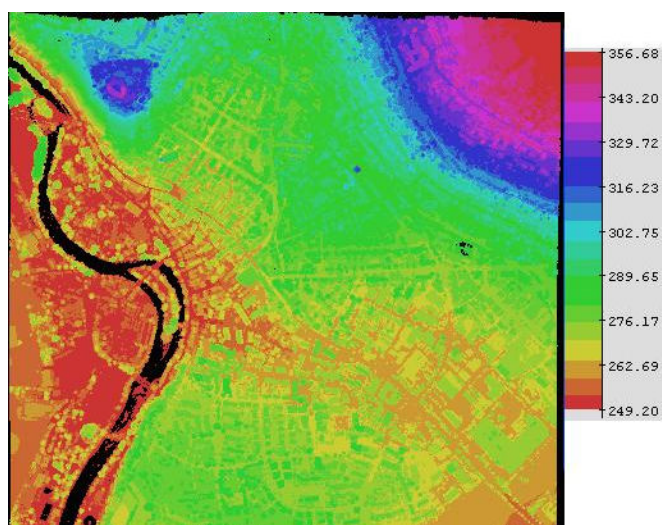


Fig3.Height variation in Lidar DSM of the whole LIDAR survey (units in meter).

C. True orthoimage generation from digital photogrammetric aerial camera

Digital aerial photographs acquired on-flight with a matricial sensor present a pronounced perspective caused by their broad field-of-view (FOV). Orthorectification is the process of geometrically adjusting a perspective image to an orthogonal image by transforming coordinates from the image space to the ground space and removing tilt and relief displacement [11]. In order to change the perspective into orthogonal projection and to formulate the topographic correction, internal and external image orientations (IO and EO) and a DEM are required [8].

The orthoimage generation process consists of five steps: interior orientation, exterior orientation, DEM generation and editing or using of existing DEM, orthoimages generation and mosaic creation [9].

In many GIS applications orthophotos are used as background information enriching their look-and-feel. Due to the characteristic having a homogeneous geometry they are often applied in order to capture data in planimetry. However, the ortho-rectification of aerial imagery is partly geometrically inaccurate and/or incomplete, i.e. buildings are distorted from their true location as they are not modeled in the DTM. [10].

Orthophotos generated with a DTM have typically following shortcoming: a-Perspective displacement and areas occluded by objects (e.g. buildings)

b- Partly geometrically inaccurate and/or incomplete orthophotos [10].

Corrective in order to avoid above mentioned effects would be the use of a Digital Surface Model (DSM) [10].

Fig.4 shows True ortho projection with a DSM.

Digital aerial photographs were orthorectified to a 8 cm spatial resolution using Lidar DSM, though they were

resampled with a bilinear convolution in order to keep the appearance of the objects represented and images were projected to the UTM coordinate system (datum WGS 84, Zone 32). After that image mosaicking were made. The whole procedure was implemented in Leica photogrammetric suite LPS digital photogrammetric workstation. Fig.5 illustrates an example of digital orthophoto resulted from orthorectification of digital photogrammetric camera image using Lidar DSM. Fig.6 shows mosaic of digital orthophotos that resulted from orthorectification of digital photogrammetric camera images using Lidar DSM.

Fig.7 shows coregistration between Lidar DSM and orthomosaic resulted from orthorectification of digital photogrammetric camera images using Lidar DSM. Swipe utility was used to check the coregistration.

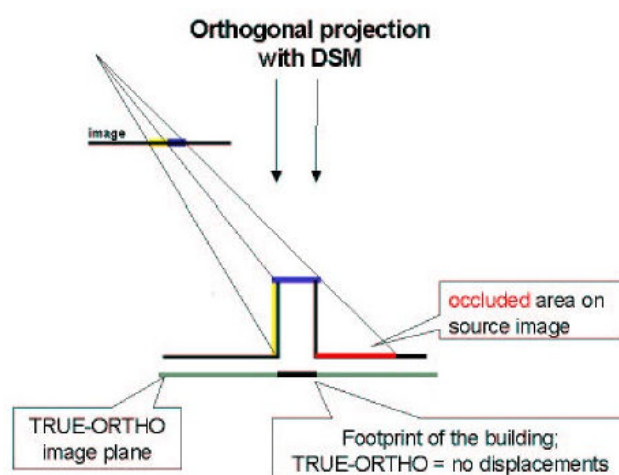


Fig 4. True ortho projection with a DSM.



Fig5. Example of digital orthophoto resulted from orthorectification of digital photogrammetric camera image using Lidar DSM.

Intensity image was used for check Point collection. The accuracy of the generated orthoimages was less than one pixel.

D. Orthoimages and radiometric equalization

Orthoimages are one of the most popular products directly derived from aerial images. In this case, from a customer's

point of view, one of the most critical aspects of orthoimages concerns their radiometry. Indeed, orthoimage creation from full-frame images is not a straightforward process when radiometric problems are taken into account. Radiometric inhomogeneities existing in raw images are related to surface Bidirectional Reflectance Distribution Function (BRDF) effects, to variation in haze composition and importance, to temporal difference between images, and so on. As a consequence, pre-processing images with radiometric corrections is required, since mosaicking them directly to obtain orthoimages mosaic would give unacceptable results, where stitches between original images are blatantly visible. Radiometric corrections were already necessary with analogue film, but they are all the more essential in a digital framework, since full-frame digital images are currently relatively small [7].



Fig.6 Mosaic of digital orthophotos that resulted from orthorectification of digital photogrammetric camera images using Lidar DSM .

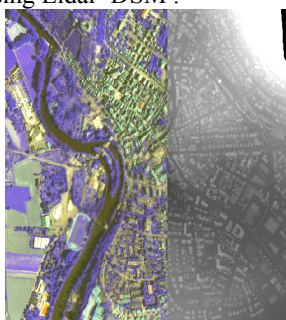


Fig.7 Overlay between Lidar DSM and orthomosaic resulted from digital photogrammetric camera.

E. LIDAR-derived metrics

Most LiDAR systems have a multiecho capability and may capture between two and five returns for every laser pulse by penetrating beyond the first reflective surfaces of the canopy[19]. In this research, first return was used to derive LIDAR-derived metrics.

First-return Contains a combination of all data classes received from the first return of each laser pulse [21].

The ultimate goal of this study was to combine LiDAR point cloud data with digital orthophoto data (raster data) as a new analysis band, LiDAR data underwent a rasterization process at the same spatial resolution as the orthophoto (8 cm)

E.1. LIDAR Intensity

In this study, first return was used to derive intensity metric. intensity image was generated from the cloud points. Lastools software was used for this purpose. Firstly .las files of the strips 3,5,7,9, and 10 have been merged using las merge module. After that las2grid was used for interpolation of the intensity data of the point cloud into grid data after that image filter (Lee) has been applied to remove noise within the intensity data. Fig.8 illustrates intensity image of the whole LIDAR survey.

A subset that correspond to the area 2 was extracted.



Fig.8 LIDAR intensity image of the whole LIDAR survey.

E.2. LIDAR Average metric

Average metric was calculated from the cloud points of the first pulse height data.

Lastools software was used for this purpose. Firstly .las files of the strips 3,5,7,9,and 10 have been merged using las merge module. After that las2grid was used for interpolation of the average metric of the point cloud into grid data.

A subset that correspond to the area 2 was extracted.

E.3. LIDAR Standard deviation metric

Standard deviation metric was calculated from the cloud points of first pulse height data.

Lastools software was used for this purpose. Firstly .las files

of the strips 3,5,7,9, and 10 have been merged using las merge module. After that las2grid was used for interpolation of the standard deviation metric of the point cloud into grid data.

A subset that correspond to the area 2 was extracted.

F. Feature detection using classification

Image classification is automatically procedures that to categorize all pixels in an image into land cover classes[18].

Classification plays an important role in the information extraction. The general classification approaches are supervised classification and unsupervised classification [17].

F.1. Maximum Likelihood Classifier

Maximum Likelihood Classifier is most widely used supervised classifier for remote sensing image processing, available in most remote sensing software. The principle of this classifier is: the probability of an object belonging to each of a predefined set of classes is calculated, and the object is then assigned to the class for which the probability is the highest [16]. In order to improve classification accuracy, different feature sets were used.

Supervised maximum likelihood classification was performed using five different feature sets. Set 1, where only the LiDAR intensity image was analyzed; Set 2, where only the spectral information of the true orthoimage was analyzed; Set 3, where the true orthoimage data were analyzed along with two LiDAR heigh metrics (average and standard deviation) ; Set 4, where two LiDAR heigh metrics (average and standard deviation) were analyzed ; Set 5, where the treatment was the same as in Set3 along with intensity image.

All the datasets were co-registered together firstly then Erdas imagine 9.2 was used for classification. Five classes were selected to represent the land use/land cover classes of the study area: buildings, roads, vegetation, water and shadows. Training samples have been collected for the five approaches .Thirty signatures have been collected in each class. The collected signatures were evaluated using histogram method, and the result is accepted before the classification process. Fig.9 shows an example of classified image using maximum likelihood classifier.

F.1.1. Separability measures

Separability measure results were slightly better when using LIDAR feature images (intensity and height) together with true orthimages. Table 2 shows average separabilities of the classes for the five approaches of the maximum likelihood classifier. In general, the computed values range from 0 to 2 where values greater than 1.9 indicate that the compared pairs have good separability, whereas very low values (less than 1) indicate that the compared spectra might be appropriate to be combined into a single one. The fifth approach has the best separability.

Fig.10 shows separabilities of the classes for the five

approaches of the maximum likelihood classifier.

Table 2: Average separabilities of the classes for the five approaches of the maximum likelihood classifier: $0 < x < 1$ (very poor separability); $1 < x < 1.9$ (poor separability); $1.9 < x < 2$ (good separability).

Features	Average Separability
Intensity	1.01
3 aerial image channels (true orthophoto)	1.56
3 aerial image channels + 2 LIDAR features	1.72
2 LIDAR features	1.32
aerial image channels+ 3 2 LIDAR features+ Intensity	1.93

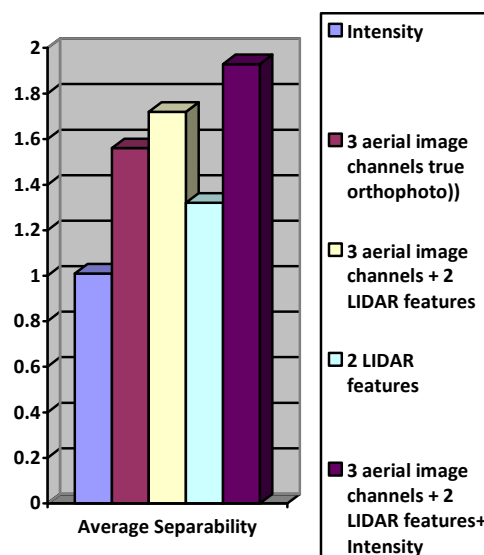


Fig.10 Average separabilities of the classes for the five approaches of the maximum likelihood classifier.

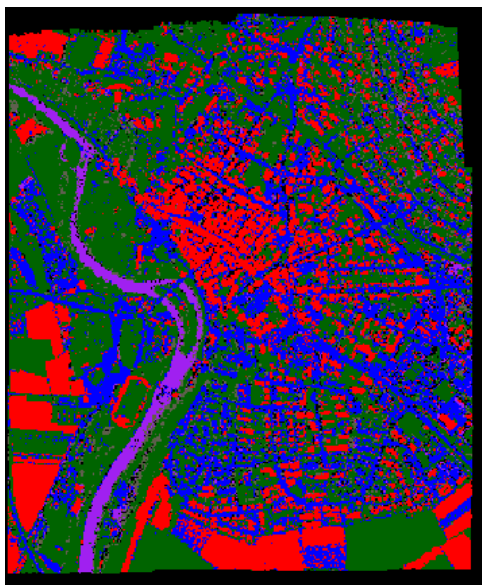


Fig.9 Example of classified image using maximum likelihood classifier.

Thematic accuracy for each approach was assessed using seventy check points.

The overall accuracy of the first approach was 60.3%, and kappa coefficient was 0.56, the overall accuracy of the second approach was 91%, and kappa coefficient was 0.82, the overall accuracy of the third approach was 93%, and kappa coefficient was 0.85, the overall accuracy of the fourth approach was 79%, and kappa coefficient was 0.76, and the overall accuracy of the last approach was 95.3%, and kappa coefficient was 0.91. After that morphological operations were performed in order to remove noise. Morphological opening with kernel size of 5×5 followed by morphological closing with kernel size of 5×5 have been used utilizing ENVI 4.8 software Table 3 indicates overall classification accuracy and kappa coefficient for the five approaches. Fig.11 illustrates overall classification accuracy and Kappa coefficient for the five approaches of the maximum likelihood classifier.

F.2. Neural network Classifier

A neural network consists of a number of interconnected nodes. Each node is simple processing element that responds to the weighted inputs it receives from other nodes [24].

The arrangement of the nodes is referred to as the network architecture. The first type of layer is the input layer, where the nodes are the element a feature vector. This vector might consist of the wave bands of a data set, the texture of the image or other more complex parameters. The second type of layer is the internal or hidden layer since it does not contain output units. There are no rules, but theory shows that one hidden layer can represent any Boolean function. An increase in the number of hidden layers enables the network to learn more complex problems, but the capacity to generalize is reduced

and there is an associated increase in training time.

Table 3. Overall classification accuracy and Kappa coefficient for the five approaches of the maximum likelihood classifier.

Features	Overall Accuracy %	Kappa coefficient
Intensity	60.3%	0.56
3 aerial image channels (true orthophoto)	91%	0.82
3 aerial image channels + 2 LIDAR features	93%	0.85
2 LIDAR features	79%	0.76
3 aerial image channels + 2 LIDAR features+ Intensity	95.3%	0.91

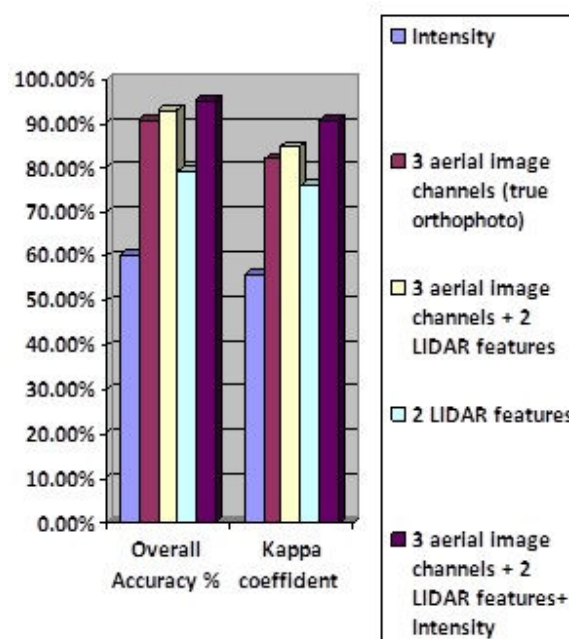


Fig.11 Overall classification accuracy and Kappa coefficient for the five approaches of the maximum likelihood classifier.

The third type of layer is the output layer and this presents the output data [26].

For image classification, the input layer is defined by the number of input data channels or feature layers whereas the output layer is defined by the number of desired classes. The network structure between these two layers consists of hidden layers with a specific number of hidden units (or neurons). The

number of hidden nodes usually defined at least as number of nodes in the input layer. Based on Kolmogorov theory, $2N+1$ hidden nodes should be used for one hidden layer (where N is number of input nodes) [23].

One of the advantages of ANNs is the possibility to integrate multi sensor data types in one classification process[25].

Other advantages are inherent with the character of neural networks: lack of assumptions about normality in datasets, ability to capture non-linearity. However, there also have several weaknesses in neural network such as slow learning rate, difficult convergence, complex network structure and ambiguous meaning of network[22].

The neural network had a feed-forward architecture with two hidden layer. The learning algorithm, was the Back-Propagation. The input layer consisted of 6 nodes, corresponding to the three digital aerial image channels, intensity image and two LIDAR feature images (average and standard deviation). The output layer was composed of 5 nodes, one for each class of the resulted five classes. ENVI 4.8 software was utilized for neural network classification. A suitable number of region of interest "ROIs" "about 30 signature" have been selected in each land cover class of the five classes. The training data for two separate classes should not overlap. Separability has been checked. The parameter of the neural network classifier has been set as number of hidden layer 2, learning rate 1, momentum 0, threshold 0.01, and number of iterations 1000, the activation function used in both layers was the sigmoid.

The overall accuracy was 97%, and kappa coefficient was 0.94.

Fig.12 Illustrates neural network RMS plot.

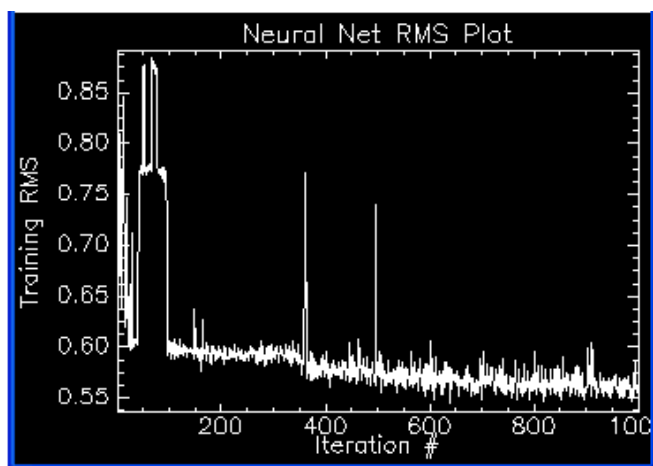


Fig.12 Neural network RMS plot.

IV. RESULTS AND DISCUSSION

LIDAR intensity was used as a feature for detection. The

LIDAR intensity image was created from the intensity values corresponding to the first return. LIDAR intensity data was integrated with photogrammetric data and LIDAR height metrics for improving the feature detection capabilities. The contribution of the individual channels has been evaluated.

Firstly the true Orthoimages were generated by true orthorectification of digital camera images using DSM from LIDAR data utilizing Leica Photogrammetric Suite (LPS) module of Erds Imagine 9.2 software for processing. The accuracy of the generated orthoimage was less than one pixel. After that orthomosaic was generated.

Secondly feature detection has been performed based on supervised classification (maximum likelihood).

Maximum likelihood classification was performed on Erdas Imagine 9.2 using five different feature sets.

The first segmentation was performed using the intensity image, the second segmentation was performed using the three digital aerial image channels whereas the third segmentation was performed using the three digital aerial image channels and two LIDAR feature images (average and standard deviation). The fourth segmentation was performed using two LIDAR feature images (average and standard deviation). The last segmentation was performed using a combination of three digital aerial image channels, intensity image and two LIDAR feature images (average and standard deviation). The separability analysis indicated that the integration of LIDAR data with photogrammetric data significantly improved the separability of classes.

Quantitative accuracy assessments of the classification results were performed. Experimental results showed that the overall accuracy and kappa statistics of the classification results were calculated for the five classifications that were performed with the five datasets. The overall accuracy of the first approach was 60.3%, and kappa coefficient was 0.56, the overall accuracy of the second approach was 91%, and kappa coefficient was 0.82, the overall accuracy of the third approach was 93%, and kappa coefficient was 0.85, the overall accuracy of the fourth approach was 79%, and kappa coefficient was 0.76, and the overall accuracy of the last approach was 95.3%, and kappa coefficient was 0.91. After that morphological operations were performed in order to remove noise.

Overall accuracy of classifications improved almost by 35% when a combination of three digital aerial image channels, intensity image and two LIDAR feature images (average and standard deviation) were used instead of intensity image only.

For detection of man-made structures, especially, by combining information from digital aerial images and Lidar data. Separability measures proved that different buildings are easier to distinguish when both aerial images and LIDAR data were used together. Overall accuracies improved about 35%. Difficulties occur in building detection by using LiDAR data only, especially due to various facilities such as antenna and rooftop structures on top of the building.

The time complexity for the computation increased with increasing number of features.

A multi-layer perceptron MLP neural network model using the back-propagation (BP) algorithm was used for improving classification results and was fed with the three digital aerial image channels combined with intensity image and two LIDAR feature images (average and standard deviation).

The overall accuracy was 97%, and kappa coefficient was 0.94. It was found that the neural network classification gives better classification accuracy than maximum likelihood classification.

V. CONCLUSIONS

The use of LIDAR intensity data for land cover classification and object recognition has been explored.

LIDAR intensity data was integrated with other ancillary data for improving the land cover classification accuracy. The contribution of the individual metrics has been evaluated.

Leica Photogrammetric Suite (LPS) workstation has been used for producing true digital orthoimages from digital aerial camera images using DSM from LIDAR data. True orthomosaic was then generated.

In this research two supervised classifiers have been used for feature detection.

In the case of supervised maximum likelihood classification different feature were incorporated in the classification procedure in order to improve the results. The classification was performed on Erdas Imagine 9.2 using three different feature sets.

In the first approach, classification was performed using the intensity image channels while in the second approach, classification was performed using the three digital aerial image channels whereas in the third approach, classification was performed using the three digital aerial image channels and two LIDAR feature images (average and standard deviation). In the fourth approach, classification was performed using two LIDAR feature images (average and standard deviation). In the last approach, classification was performed using a combination of three digital aerial image channels, intensity image and two LIDAR feature images (average and standard deviation).

It was found that the last approach is the best followed by the third approach then the second approach then the fourth approach followed by the first approach.

In the case of a multi-layer perceptron MLP neural network classification, a combination of three digital aerial image channels, intensity image and two LIDAR feature images (average and standard deviation) were used.

Regarding the two classifiers, neural network outperforms maximum likelihood classification.

It is recommended to assess the effect of normalizing intensity data using geometric characteristics (angle and distance) on feature detection.

ACKNOWLEDGEMENT

Vaihingen data set was provided by the German Society for Photogrammetry, Remote Sensing and Geoinformation (DGPF) [Cramer, 2010]:<http://www.ifp.uni-stuttgart.de/dgpf/DKEP-Allg.html> (in German) The author thanks them for giving her the data. The editing and comments of the reviewers is gratefully appreciated.

REFERENCES

- [1] N. Demir, D. Poli, and E. Baltsavias, "Extraction of buildings and tree using images and LIDAR data", *The International Archives of the Photogrammetry, Remote Sensing and Spatial Information Sciences*, vol. XXXVII. Part B4. Beijing, 2008
- [2] N. Haala, M. Cramer, and K. Jacobsen, "The German camera evaluation project - results from the geometry group" Available:http://www.ifp.uni-stuttgart.de/publications/2010/Calgary_Haala_Cramer_Jacobsen.pdf, 2010
- [3] C. Heipke, K. Jacobsen, and J. Mills, "Theme issue: "Digital aerial cameras" *ISPRS Journal of Photogrammetry & Remote Sensing*, vol. 60, 2006, pp 361–362
- [4] M. Cramer, "10 Years IFP Test Site Vaihingen/Enz: An Independent Performance Study", 50 photogrammetric Week, Stuttgart, Wichmann Ed., 2005, pp. 89-106.
- [5] C. Lemaire, "Aspects of the DSM production with high resolution images", *The International Archives of the Photogrammetry, Remote Sensing and Spatial Information Sciences*, vol. XXXVII. Part B4, Beijing, 2008
- [6] J. Kunapo, "Spatial data integration for classification of 3D point clouds from digital photogrammetry" *APPLIED GIS*, vol 1, no. 3, 2005 MONASH UNIVERSITY EPRESS
- [7] N. Paparoditis, J. Souchon, G. Martinoty, and M. Deseilligny, "High-end aerial digital cameras and their impact on the automation and quality of the production workflow", *International Society for Photogrammetry and Remote Sensing Inc. (ISPRS)*, 2006, Published by Elsevier B.V.
- [8] R. Valbuena, F. Mauro, F. J. Arjonilla, and J. A. Manzanera, "Comparing airborne laser scanning imagery fusion methods based on geometric accuracy in forested areas" *Remote Sensing of Environment* 115, 2011, pp. 1942–1954
- [9] I. Sebari, H. Lahmami, and M. Ettarid, "Assessment and comparison of the quality of digital ortho-images generated from digital aerial images and from scanned analogue aerial images", *FIG Working Week 2011 Marrakech, Morocco*, 18-22 May, 2011
- [10] K. Lothhammer, "State-of-the-art photogrammetric workflow the inpho approach", *Semana Geomatica*, IGAC Bogotá, Colombia, 2005
- [11] X. Liu, Z. Zhang, J. Peterson, and S. Chandra, "LiDAR-Derived High Quality Ground Control Information and DEM for Image Orthorectification" *Geoinformatica 11* 2007, pp. 37–53 DOI 10.1007/s10707-006-0005-9

- [12] M. García, D. Riaño, E.Chuvieco, and F. M. Danson “Estimating biomass carbon stocks for a Mediterranean forest in central Spain using LiDAR height and intensity data”, *Remote Sensing of Environment* 114, 2010, pp. 816–830
- [13] A.S. Antonarakis, K.S.Richards, and J. Brasington “Object-based land cover classification using airborne LiDAR”, *Remote Sensing of Environment* 112 , 2008, pp. 2988–2998
- [14] W. Y.Yan, A.Shaker, A. Habib, and A. P. Kersting “Improving classification accuracy of airborne LiDAR intensity data by geometric calibration and radiometric correction”, *ISPRS Journal of Photogrammetry and Remote Sensing*, 67 ,2012, pp.35–44
- [15] M. Chen, W. Su, L. LI, C. Zhang, A. Yue, and H. Li, “A Comparison of Pixel-based and Object-oriented Classification Using SPOT5 Imagery” ,*Proceedings of the 13th WSEAS International Conference on Applied Mathematics (MATH'08)*,2008
- [16] W. Su, C. Zhang, L. Li, Y. Wang, and D. Li “Object oriented implementation monitoring of zone type land consolidation engineering using SPOT 5 imagery” , 7th WSEAS Int. Conf. on Applied Computer & Applied Computational Science (ACACOS '08), Hangzhou, China, April 6-8, 2008
- [17] A. Yue, S.Weii, D. Li, C. Zhang, and Y. Huang, “Texture Feature Extraction for Land-cover Classification of Remote Sensing Data in Land Consolidation District Using Semi-variogram” , 7th WSEAS Int. Conf. on APPLIED Computer & Applied Computational Science (ACACOS '08), Hangzhou, China, April 6-8, 2008
- [18] S. Chitwong, S. Witthayapradit, S. Intajag, and F. Cheevasuvit, “Multispectral image classification using back-propagation neural network in PCA domain”, Available: <http://www.wseas.us/e-library/conferences/brazil2004/papers/489-511.pdf>
- [19] D. Jaskierniak, P. N.J. Lane, A. Robinson, and A. Lucieer, “Extracting LiDAR indices to characterise multilayered forest structure using mixture distribution functions”, *Remote Sensing of Environment* 115 ,2011 pp.,573–585 Available : www.sciencedirect.com
- [20] G. Chust, I.Galpársoro, A. Borja, J. Franco, and A. Uriarte, “Coastal and estuarine habitat mapping, using LIDAR height and intensity and multi-spectral imagery”, *Estuarine, Coastal and Shelf Science* 78 , 2008, pp. 633-643 Available : www.sciencedirect.com
- [21] V. Archana , M. Deborah, and S. P. Sivani “Building Extraction from LiDAR Data”,*Geospatial world forum* ,Hyderabad, India ,18-20 january 2011
- [22] H. Xiao , X. Zhang, Y. Du, “A Comparison of Neural Network, Rough Sets and Support Vector Machine on Remote Sensing Image Classification”, 7th WSEAS Int. Conf. on Applied Computer & Applied Computational Science (ACACOS '08), Hangzhou, China, April 6-8, 2008
- [23] Y. Rangsaneri, P. Thitimajshima , and S. Promcharoen”A Study of Neural Network Classification of Jers-1/Ops Images. ”,ACRS 1998, Available: http://www.geospatialworld.net/index.php?option=com_content&view=article&id=14438&catid=89%3Atechnology-image-processing&Itemid=50
- [24] P. N. Dadhich1 and S. Hanaoka ”Markov Method Integration with Multi-layer Perceptron Classifier for Simulation of Urban Growth of Jaipur City”, selected topics in power systems and remote sensing,ISBN: 978-960-474-233-2, ISSN: 1792-5088
- [25] A.C.Bernard, G.G.Wilkinson, and I.Kanellopoulos “Training for neural network soft classification of remotely sensed imagery “*Int.j.Remote Sensing* , 1997 vol.18,no.8,pp.1851-1856
- [26] P.M.Atkinson and A.R.L.Tatnall , “Neural networks in remote sensing”, *Int.j.Remote Sensing* , vol.18,no.4 , 1997 , pp.699-709